HHS Public Access

Author manuscript

ACS Catal. Author manuscript; available in PMC 2024 July 07.

Published in final edited form as:

ACS Catal. 2023 July 07; 13(13): 9018–9024. doi:10.1021/acscatal.3c01984.

CdS Quantum Dots for Metallaphotoredox-Enabled Cross-Electrophile Coupling of Aryl Halides with Alkyl Halides

Julianna M. Mouat[†], **Jonas K. Widness**[†], **Daniel G. Enny**[†], **Mahilet T. Meidenbauer**[‡], **Farwa Awan**[§], **Todd D. Krauss**[*,§,^], **Daniel J. Weix**[*,†]

[†]Department of Chemistry, University of Wisconsin-Madison, 1101 University Ave, Madison, WI 53706 USA

[‡]Materials Science Program, University of Rochester, Rochester, NY 14627 USA

[§]Department of Chemistry, University of Rochester, Rochester, NY 14627 USA

[^]Institute of Optics, University of Rochester, Rochester, NY 14627 USA

Abstract

Semiconductor quantum dots (QDs) offer many advantages as photocatalysts for synthetic photoredox catalysis, but no reports have explored the use of QDs with nickel catalysts for C-C bond formation. We show here that 5.7 nm CdS QDs are robust photocatalysts for photoredox-promoted cross-electrophile coupling (40 000 TON). These conditions can be utilized on small scale (96-well plate) or adapted to flow. NMR studies show that triethanolamine (TEOA) capped QDs are the active catalyst and that TEOA can displace native phosphonate and carboxylate ligands, demonstrating the importance of QD surface chemistry.

Graphical Abstract

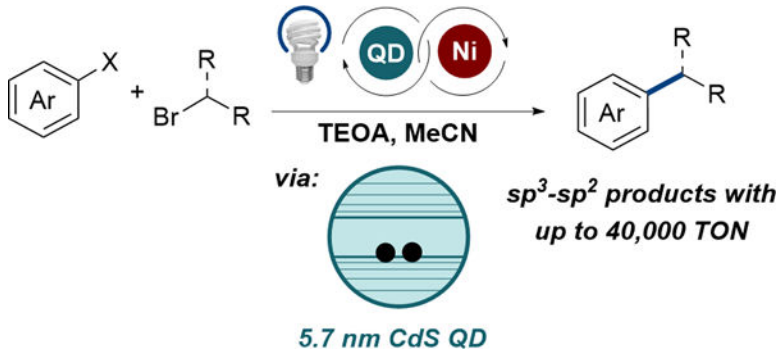

[*]Corresponding Author: dweix@wisc.edu, todd.krauss@rochester.edu.

ASSOCIATED CONTENT

SUPPORTING INFORMATION

Additional optimization and characterization data, experimental procedures, and characterization data for all isolated compounds (PDF). This material is available free of charge via the Internet at http://pubs.acs.org.

Keywords

quantum dot; nanoplatelet; nickel; cross-electrophile coupling; C–C bond formation; photochemistry

Photoredox chemistry employing transition metal co-catalysts is a powerful strategy for C-C bond formation,[1–3] but is generally limited by a small number of photoredox catalysts. For example, photoredox-promoted cross-electrophile coupling (PPXEC) procedures commonly require iridium-based dyes, and stoichiometric use of expensive and high MW silane reductants, or both (Scheme 1A).[4–11] Despite this, PPXEC is widely utilized on small-scale and would be an attractive approach to large-scale XEC if costs could be decreased. Both Vannucci's and Lei's PPXEC approaches avoided the need for silane reagents, which can be expensive and often introduce purification challenges, but required Ir dyes.[12,13] Precious metal dyes are among the most developed metallaphotoredox catalysts, yet there are concerns surrounding the security of the platinum-group metal supply[14] and expense of these dyes at large scale. Recent reports have introduced organophotocatalysts, sometimes alongside non-silane reductants,[15–18] but these catalysts are also expensive for large scale use and often require higher catalyst loadings. There is a need for scalable PPXEC catalysts that do not suffer from these hurdles.

Our group and others have evaluated semiconductor quantum dots (QDs) as replacements for precious-metal dyes in a variety of photoredox[19–23] and redox-neutral metallaphotoredox reactions,[20,24–26] but their viability for reductive metallaphotoredox catalysis remains unexplored (Scheme 1B). QDs could be an ideal replacement for precious metals and organic dyes due to their tunable visible absorption,[27] large molar absorptivity coefficients[28], well-defined syntheses from inexpensive precursors[29,30], solution stability in organic solvents, and high photostability[31–33], among other advantages.[34–38] However, we envisioned several challenges in realizing a QD-catalyzed PPXEC reaction. The low concentrations of QDs typically employed,[39,40] combined with shorter excited-state lifetimes[41–43] could give sluggish bimolecular quenching with a metal co-catalyst. Second, QDs can bind or react with metal ions[44–46] and common organic functional groups,[47–49] and undesired side reactivity between the QDs, metal co-catalysts, and reactants could inhibit catalysis. Finally, given the wide array of available QDs and nanomaterials,[30] the choice of appropriate nanomaterial composition and morphology was not obvious. We report here a systematic investigation of the use of QDs in a model PPXEC reaction that illustrates CdS QDs are as effective as small-molecule dyes (Scheme 1C). Binding studies reveal that the terminal reductant (triethanolamine), a reported QD ligand,[50–53] replaces the native QD ligands in-situ, remodeling the QD surface for optimal reactivity.

To identify the optimal nanomaterial photocatalysts for PPXEC, we examined of several nanomaterials (reported in mol% of nanomaterial) of differing morphologies, sizes, and electronic/chemical characteristics (See Supporting Information Section 2 for characterization details).[20,54–61] 5.7 nm CdS QDs(size determined by TEM imaging, see Supporting Information Section 2 for sizing details) were the most effective photocatalyst for this transformation (~40,000 TON), while smaller CdS QDs gave lower yields of

product and more dehalogenated arene (Table 1, entries 1–4). Employing higher-energy 390 nm irradiation to better excite 3.9 nm CdS QDs was also detrimental (Table 1, entries 5–6). Because dehalogenation has been associated with over-reduction of arylnickel(II) intermediates,[62] the increased amount of dehalogenation observed with smaller diameter QDs suggests that larger bandgap energies play a negative role. On the other hand, among different sized CdS QDs, the increased yield does not appear to be due absorbance of more photons (see Supporting Information Figure 2.6). Overall, a number of size-dependent factors may account for the superior performance of the larger 5.7 nm CdS QDs compared to the other nanomaterials, including the extinction coefficients, band edge positions, and ligand coverage.

CdSe QDs, which exhibit smaller band gaps and lower valence band potentials than CdS,[27,63] did not provide the product in any appreciable yield (Table 1, entries 7–8), possibly due to insufficient driving force required for efficient oxidation of amine reductants. Both bulk and nanocrystalline $CsPbBr_3$ perovskites, possessing similar band gaps to 5.7 nm CdS were completely ineffective (Table 1, entries 9–10), likely due to their rapid dissolution in polar environments unless functionalized with stabilizing ligands,[60] highlighting a fundamental challenge in the use of perovskite photocatalysts for organic chemistry. Preliminary attempts to use ~4.5 monolayer (ML) CdSe and CdS nanoplatelets, unexplored materials for metallaphotoredox catalysis, afforded promising yields (Table 1, entries 11–14) with very high total TONs (in some cases, > 500 000 see Supporting Information Section 5 for details). While more concentrated NPL solutions were problematic, comparison of NPLs with QDs at the same (lower) concentration demonstrated that NPLs can be more productive per particle (see Supporting Information Table S5). Owing to the greater synthetic complexity of nanoplatelets[64] and their lower initial performance, we opted to continue using 5.7 nm CdS QDs in this study. However, the high molar productivity of nanoplatelets suggests their significant potential as photoredox catalysts in future applications.

The optimized conditions employ $NiCl_2$(dme) with terpyridine as a ligand for Ni, utilizing triethanolamine (TEOA) as a homogeneous terminal reductant, with 5.7 nm CdS QDs (2.0×10^{-3} mol%) and blue LEDs. Reducing the loading of Ni/ligand or reductant produced diminished yields (Table 2, entries 1–3). Use of alternative tertiary amine reductants instead of TEOA gave greatly diminished yields despite exhibiting similar oxidation potentials[65–68] (Table 2, entries 4–7). Furthermore, the steady-state photoluminescence of the QDs was quenched to a greater extent by TEOA than DIPEA or Et_3N (Supporting Information Section 5.2), consistent with its superior performance. Lowering the QD loading was detrimental, while bulk CdS powder was not an effective photocatalyst (Table 2, entries 8–9). Control experiments verified that all components were all necessary for product formation. (Table 2, entry 10).

We then briefly investigated the compatibility of the CdS QD/TEOA system with synthetically relevant substrates (Scheme 2). Electron-rich and neutral aryl iodides were cross-coupled in good yields (**3a-3c**), while heteroaryl iodides including pyridine, indole, pyrazole, and indazole (**3g-3j**) could also be coupled. When electron-poor aryl iodides were used, significant amounts of hydrodehalogenated product were observed, consistent with the ability of CdX QDs (X = S, Se) to directly reduce electron poor aryl iodides.[69]

Electron-poor aryl bromides could also be coupled, albeit requiring 1.5 equivalents of Ar-Br to achieve good yields (**3d-3f**). Following this trend, electron poor heteroaryl moieties, including pyridine (**3q**) and pyrimidine (**3r, 3s**)**,** could be coupled in moderate yield. Additionally, both primary (**3a**-**3l**, **3o**, **3p**) and secondary alkyl bromides (**3m, 3n, 3t, 3u**) could be coupled using this method. Synthetically valuable moieties including halides, nitriles, ketones, esters, protected amines were generally well-tolerated. Corey lactone-derived **3o** and uridine-derived **3p** were afforded in good yields without epimerization of chiral centers.

In the optimized reaction (Table 1, entry 1), the remainder of the mass balance was primarily Protodehalogenation (Ph–H) with small amounts of remaining starting material and alkyl dimer. For the lower-yielding reactions in Scheme 2, protodehalogenation and alkyl dimerization were the main side products. For less reactive aryl halides, substantial amounts of the aryl halide remained.

The advantages of inexpensive production and robust solution stability render QDs an ideal photocatalyst platform for large-scale applications.[70] We found that **3l** could be scaled up to 5 mmol scale on the benchtop in batch and **3c** could be scaled to 7.5 mmol in a flow reactor (Scheme 2). The latter reaction used only 0.001 mol% QDs (corresponding to a material cost of $0.26, see Supporting Information Section 3.4 for details).

Furthermore, the reaction conditions could be readily applied to a smaller-scale, high-throughput format, utilizing a commercial 96 well-plate equipped with a blue LED array on a shaker plate (see Supporting Information Section 3.2 for details regarding set up and heat map data).

Modulation of the QD ligand environment by precursory exchange or in-situ interactions with reaction components is known to strongly impact catalysis by changing the permeability of the ligand sphere.[71–74] To determine whether TEOA enables optimal QD performance through surface modification, we monitored for displacement of native oleate ligands from the QD surface upon treatment with TEOA via ^{1}H NMR (Figure 1). Alcohols have been proposed to undergo X-type ligand exchange with carboxylate QD ligands,[75] but are not commonly employed as capping ligands for QDs.[76–78] Triethanolamine has been explored as a water-solubilizing ligand for QDs in sensing applications,[50,51] however ligand exchange dynamics and photocatalysis with TEOA-capped QDs have not been explored. Our ^{1}H NMR study showed oleate displacement from the QD surface by TEOA upon addition of TEOA equivalencies well below that of the catalytic reaction (Figures S4 and S7). Meanwhile, Et3N and DIPEA displaced only a small fraction of oleates on the QD surface (Figure S8). TEOA also displaced undec-10-en-1-ylphosphonic acid (UDPA) ligands from CdS (Figure S5). UDPA is known to bind more strongly than carboxylates to Cd sites on QD surfaces.[79] This similar efficacy of displacement together with TEOA's ability to form stable Cd(II) chelates[80] suggests that TEOA may remove ligands by chelation and stripping of surface bound CdX2 (X = UDPA or oleate) complexes, rather than undergoing X-type ligand exchange.[81,82] Accompanying oleate displacement, a large negative nuclear Overhauser effect (NOE) correlation was observed between the methylene resonances of TEOA in the presence of QDs, indicating their dynamic association with the exposed QD

surface following the displacement of surface-bound Cd(oleate)2 (Figure S7).[83] While the binding mode of TEOA to the QD surface in this particular system remains unknown, (i.e., L vs X-type, binding through the amine vs hydroxyl moieties), our experiments are consistent with in-situ formation of TEOA-capped QDs as the active catalyst under the optimal conditions (Figure 1). Structurally similar tertiary amines bearing zero or one hydroxyl group were less effective reductants, but two hydroxyl groups provided similar results (Table 2, entries 4–7), suggesting that some level of chelation is critical to function as a surface-remodeling reductant.[84]

In conclusion, we have demonstrated how CdS QDs with TEOA constitute a cost-effective photoreduction system for Ni-mediated cross-electrophile coupling that demonstrates a broad scope and good scalability. NMR studies illustrate the role of TEOA as a surface-binding reductant and how surface remodeling could be used to improve reductive chemistry with QDs. Continuing studies on the use of nanomaterials for organic synthesis are ongoing and will be reported in due course.

Supplementary Material

Refer to Web version on PubMed Central for supplementary material.

ACKNOWLEDGMENT

This work was supported by the NIH (R21GM141622 to D.J.W. and T.D.K.), the NSF (CHE-1904847 to T.D.K.), the University of Wisconsin-Madison (D.J.W.), and the donors to the Wayland E. Noland Chair (D.J.W.). The instrumentation in the PBCIC was supported as follows: Thermo Q Extractive Plus was supported by the NIH (no. 1S10 OD020022); Shimadzu GCMS-QP2010S was supported by the Department of Chemistry; and Bruker Avance III 500 was supported by a generous gift from Paul J. and Margaret M. Bender. The authors thank the Yoon group (UW-Madison) for helpful discussions about photoluminescence quenching experiments, and for access to their chemical inventory and supplies. They also thank Prof. Jillian Dempsey, Jennica Kelm, and Christian Dones-LaSalle (University of North Carolina-Chapel Hill) for guidance with NMR experiments.

REFERENCES

1. Chan AY; Perry IB; Bissonnette NB; Buksh BF; Edwards GA; Frye LI; Garry OL; Lavagnino MN; Li BX; Liang Y; Mao E; Millet A; Oakley JV; Reed NL; Sakai HA; Seath CP; MacMillan DWC Metallaphotoredox: The Merger of Photoredox and Transition Metal Catalysis. Chem. Rev 2022, 122, 1485–1542. [PubMed: 34793128]
2. Hopkinson MN; Sahoo B; Li J-L; Glorius F Dual Catalysis Sees the Light: Combining Photoredox with Organo-, Acid, and Transition-Metal Catalysis. Chem. – Eur. J 2014, 20, 3874–3886. [PubMed: 24596102]
3. Prier CK; Rankic DA; MacMillan DWC Visible Light Photoredox Catalysis with Transition Metal Complexes: Applications in Organic Synthesis. Chem. Rev 2013, 113, 5322–5363. [PubMed: 23509883]
4. Sakai HA; Liu W; Le C “Chip”; MacMillan, D. W. C. Cross-Electrophile Coupling of Unactivated Alkyl Chlorides. J. Am. Chem. Soc 2020, 142, 11691–11697. [PubMed: 32564602]
5. Zhang P; Le C “Chip”; MacMillan, D. W. C. Silyl Radical Activation of Alkyl Halides in Metallaphotoredox Catalysis: A Unique Pathway for Cross-Electrophile Coupling. J. Am. Chem. Soc 2016, 138, 8084–8087. [PubMed: 27263662]
6. Smith RT; Zhang X; Rincón JA; Agejas J; Mateos C; Barberis M; García-Cerrada S; de Frutos O; MacMillan DWC Metallaphotoredox-Catalyzed Cross-Electrophile C sp 3 –C sp 3 Coupling of Aliphatic Bromides. J. Am. Chem. Soc 2018, 140, 17433–17438. [PubMed: 30516995]

7. Delgado P; Glass RJ; Geraci G; Duvadie R; Majumdar D; Robinson RI; Elmaarouf I; Mikus M; Tan KL Use of Green Solvents in Metallaphotoredox Cross-Electrophile Coupling Reactions Utilizing a Lipophilic Modified Dual Ir/Ni Catalyst System. J. Org. Chem 2021, 86, 17428–17436. [PubMed: 34808052]
8. Juliá F; Constantin T; Leonori D Applications of Halogen-Atom Transfer (XAT) for the Generation of Carbon Radicals in Synthetic Photochemistry and Photocatalysis. Chem. Rev 2022, 122, 2292–2352. [PubMed: 34882396]
9. Dewanji A; Bülow RF; Rueping M Photoredox/Nickel Dual-Catalyzed Reductive Cross Coupling of Aryl Halides Using an Organic Reducing Agent. Org. Lett 2020, 22, 1611–1617. [PubMed: 32011897]
10. Kerackian T; Reina A; Bouyssi D; Monteiro N; Amgoune A Silyl Radical Mediated Cross-Electrophile Coupling of N-Acyl-Imides with Alkyl Bromides under Photoredox/Nickel Dual Catalysis. Org. Lett 2020, 22, 2240–2245. [PubMed: 32148046]
11. Yu W; Chen L; Tao J; Wang T; Fu J Dual Nickel- and Photoredox-Catalyzed Reductive Cross-Coupling of Aryl Vinyl Halides and Unactivated Tertiary Alkyl Bromides. Chem. Commun 2019, 55, 5918–5921.
12. Paul A; Smith MD; Vannucci AK Photoredox-Assisted Reductive Cross-Coupling: Mechanistic Insight into Catalytic Aryl–Alkyl Cross-Couplings. J. Org. Chem 2017, 82, 1996–2003. [PubMed: 28112920]
13. Duan Z; Li W; Lei A Nickel-Catalyzed Reductive Cross-Coupling of Aryl Bromides with Alkyl Bromides: Et3N as the Terminal Reductant. Org. Lett 2016, 18, 4012–4015. [PubMed: 27472556]
14. Volz D; Wallesch M; Fléchon C; Danz M; Verma A; Navarro JM; Zink DM; Bräse S; Baumann T From Iridium and Platinum to Copper and Carbon: New Avenues for More Sustainability in Organic Light-Emitting Diodes. Green Chem 2015, 17, 1988–2011.
15. Luridiana A; Mazzarella D; Capaldo L; Rincón JA; García-Losada P; Mateos C; Frederick MO; Nuño M; Jan Buma W; Noël T The Merger of Benzophenone HAT Photocatalysis and Silyl Radical-Induced XAT Enables Both Nickel-Catalyzed Cross-Electrophile Coupling and 1,2-Dicarbofunctionalization of Olefins. ACS Catal 2022, 12, 11216–11225. [PubMed: 36158902]
16. Lau SH; Borden MA; Steiman TJ; Wang LS; Parasram M; Doyle AG Ni/Photoredox-Catalyzed Enantioselective Cross-Electrophile Coupling of Styrene Oxides with Aryl Iodides. J. Am. Chem. Soc 2021, 143, 15873–15881. [PubMed: 34542286]
17. Yedase GS; Jha AK; Yatham VR Visible-Light Enabled C(s p 3)–C(s p 2) Cross-Electrophile Coupling via Synergistic Halogen-Atom Transfer (XAT) and Nickel Catalysis. J. Org. Chem 2022, 87, 5442–5450. [PubMed: 35357838]
18. Tian X; Kaur J; Yakubov S; Barham JP α-Amino Radical Halogen Atom Transfer Agents for Metallaphotoredox-Catalyzed Cross-Electrophile Couplings of Distinct Organic Halides. ChemSusChem 2022, 15, e202200906. [PubMed: 35587725]
19. Widness JK; Enny DG; McFarlane-Connelly KS; Miedenbauer MT; Krauss TD; Weix DJ CdS Quantum Dots as Potent Photoreductants for Organic Chemistry Enabled by Auger Processes. J. Am. Chem. Soc 2022, 144, 12229–12246. [PubMed: 35772053]
20. Caputo JA; Frenette LC; Zhao N; Sowers KL; Krauss TD; Weix DJ General and Efficient C–C Bond Forming Photoredox Catalysis with Semiconductor Quantum Dots. J. Am. Chem. Soc 2017, 139, 4250–4253. [PubMed: 28282120]
21. Huang C; Li X-B; Tung C-H; Wu L-Z Photocatalysis with Quantum Dots and Visible Light for Effective Organic Synthesis. Chem. – Eur. J 2018, 24, 11530–11534. [PubMed: 29575190]
22. Wu H-L; Qi M-Y; Tang Z-R; Xu Y-J Semiconductor Quantum Dots: A Versatile Platform for Photoredox Organic Transformation. J. Mater. Chem. A 2023, 11, 3262–3280.
23. Yuan Y; Jin N; Saghy P; Dube L; Zhu H; Chen O Quantum Dot Photocatalysts for Organic Transformations. J. Phys. Chem. Lett 2021, 12, 7180–7193. [PubMed: 34309389]
24. Zhang Z; Rogers CR; Weiss EA Energy Transfer from CdS QDs to a Photogenerated Pd Complex Enhances the Rate and Selectivity of a Pd-Photocatalyzed Heck Reaction. J. Am. Chem. Soc 2020, 142, 495–501. [PubMed: 31820964]

25. Zhao Z; Reischauer S; Pieber B; Delbianco M Carbon Dot/TiO2 Nanocomposites as Photocatalysts for Metallaphotocatalytic Carbon–Heteroatom Cross-Couplings. Green Chem 2021, 23, 4524–4530.
26. Zhao Z; Pieber B; Delbianco M Modulating the Surface and Photophysical Properties of Carbon Dots to Access Colloidal Photocatalysts for Cross-Couplings. ACS Catal 2022, 12, 13831–13837.
27. Jasieniak J; Califano M; Watkins SE Size-Dependent Valence and Conduction Band-Edge Energies of Semiconductor Nanocrystals. ACS Nano 2011, 5, 5888–5902. [PubMed: 21662980]
28. Sun J; Goldys EM Linear Absorption and Molar Extinction Coefficients in Direct Semiconductor Quantum Dots. J. Phys. Chem. C 2008, 112, 9261–9266.
29. Reiss P; Carrière M; Lincheneau C; Vaure L; Tamang S Synthesis of Semiconductor Nanocrystals, Focusing on Nontoxic and Earth-Abundant Materials. Chem. Rev 2016, 116, 10731–10819. [PubMed: 27391095]
30. Alivisatos AP Semiconductor Clusters, Nanocrystals, and Quantum Dots. Science 1996, 271, 933.
31. Soloviev M Nanoparticles in Biology and Medicine: Methods and Protocols; Springer US: New York, NY, 2020.
32. Resch-Genger U; Grabolle M; Cavaliere-Jaricot S; Nitschke R; Nann T Quantum Dots versus Organic Dyes as Fluorescent Labels. Nat. Methods 2008, 5, 763–775. [PubMed: 18756197]
33. Gould TJ; Bewersdorf J; Hess ST A Quantitative Comparison of the Photophysical Properties of Selected Quantum Dots and Organic Fluorophores. Z. Für Phys. Chem 2008, 222, 833–849.
34. Photocatalytic systems based on heterogeneous semiconductors constitute another promising platform for overcoming limitations of small-molecule photocatalysts See the following references:
35. Gisbertz S; Pieber B Heterogeneous Photocatalysis in Organic Synthesis. ChemPhotoChem 2020, 4, 456–475.
36. Dam B; Das B; Patel BK Graphitic Carbon Nitride Materials in Dual Metallo-Photocatalysis: A Promising Concept in Organic Synthesis. Green Chem 2023, 25, 3374–3397.
37. Savateev A; Antonietti M Heterogeneous Organocatalysis for Photoredox Chemistry. ACS Catal 2018, 8, 9790–9808.
38. Marchi M; Gentile G; Rosso C; Melchionna M; Fornasiero P; Filippini G; Prato M The Nickel Age in Synthetic Dual Photocatalysis: A Bright Trip Toward Materials Science. ChemSusChem 2022, 15, e202201094. [PubMed: 35789214]
39. Arcudi F; Đorđević L; Nagasing B; Stupp SI; Weiss EA Quantum Dot-Sensitized Photoreduction of CO2 in Water with Turnover Number > 80,000. J. Am. Chem. Soc 2021, 143, 18131–18138. [PubMed: 34664969]
40. Feng Y-X; Wang H-J; Wang J-W; Zhang W; Zhang M; Lu T-B Stand-Alone CdS Nanocrystals for Photocatalytic CO2 Reduction with High Efficiency and Selectivity. ACS Appl. Mater. Interfaces 2021, 13, 26573–26580. [PubMed: 34038075]
41. Mi C; Saniepay M; Beaulac R Overcoming the Complex Excited-State Dynamics of Colloidal Cadmium Selenide Nanocrystals Involved in Energy Transfer Processes. Chem. Mater 2018, 30, 5714–5725.
42. Pu C; Qin H; Gao Y; Zhou J; Wang P; Peng X Synthetic Control of Exciton Behavior in Colloidal Quantum Dots. J. Am. Chem. Soc 2017, 139, 3302–3311. [PubMed: 28170239]
43. Gammon D; Snow ES; Katzer DS Excited State Spectroscopy of Excitons in Single Quantum Dots. Appl. Phys. Lett 1995, 67, 2391–2393.
44. Jong T; Parry DL Adsorption of Pb(II), Cu(II), Cd(II), Zn(II), Ni(II), Fe(II), and As(V) on Bacterially Produced Metal Sulfides. J. Colloid Interface Sci 2004, 275, 61–71. [PubMed: 15158381]
45. Hörner G; Johne P; Künneth R; Twardzik G; Roth H; Clark T; Kisch H Semiconductor Type A Photocatalysis: Role of Substrate Adsorption and the Nature of Photoreactive Surface Sites in Zinc Sulfide Catalyzed C–C Coupling Reactions. Chem. – Eur. J 1999, 5, 208–217.
46. Davis AP; Hsieh YH; Huang CP Photo-Oxidative Dissolution of CdS(s): The Effect of Cu(II) Ions. Chemosphere 1994, 28, 663–674.

47. Hines DA; Kamat PV Quantum Dot Surface Chemistry: Ligand Effects and Electron Transfer Reactions. J. Phys. Chem. C 2013, 117, 14418–14426.

48. Kessler ML; Starr HE; Knauf RR; Rountree KJ; Dempsey JL Exchange Equilibria of Carboxylate-Terminated Ligands at PbS Nanocrystal Surfaces. Phys. Chem. Chem. Phys 2018, 20, 23649–23655. [PubMed: 30191247]

49. Chen PE; Anderson NC; Norman ZM; Owen JS Tight Binding of Carboxylate, Phosphonate, and Carbamate Anions to Stoichiometric CdSe Nanocrystals. J. Am. Chem. Soc 2017, 139, 3227–3236. [PubMed: 28125780]

50. Yan XQ; Shang ZB; Zhang Z; Wang Y; Jin WJ Fluorescence Sensing of Nitric Oxide in Aqueous Solution by Triethanolamine-Modified CdSe Quantum Dots. Luminescence 2009, 24, 255–259. [PubMed: 19294661]

51. Shang ZB; Wang Y; Jin WJ Triethanolamine-Capped CdSe Quantum Dots as Fluorescent Sensors for Reciprocal Recognition of Mercury (II) and Iodide in Aqueous Solution. Talanta 2009, 78, 364–369. [PubMed: 19203596]

52. Dlamini NN; Rajasekhar Pullabhotla VSR; Revaprasadu N Synthesis of Triethanolamine (TEA) Capped CdSe Nanoparticles. Mater. Lett 2011, 65, 1283–1286.

53. Dlamini NN; Pullabhotla VSRR; Revaprasadu N A Simple Route to Triethanolamine (TEA) and Cysteine Capped ZnSe Nanoparticles. J. Nanosci. Nanotechnol 2012, 12, 2645–2651. [PubMed: 22755103]

54. Liu Y-Y; Liang D; Lu L-Q; Xiao W-J Practical Heterogeneous Photoredox/Nickel Dual Catalysis for C–N and C–O Coupling Reactions. Chem. Commun 2019, 55, 4853–4856.

55. Li J-Y; Li Y-H; Qi M-Y; Lin Q; Tang Z-R; Xu Y-J Selective Organic Transformations over Cadmium Sulfide-Based Photocatalysts. ACS Catal 2020, 10, 6262–6280.

56. Li X-B; Li Z-J; Gao Y-J; Meng Q-Y; Yu S; Weiss RG; Tung C-H; Wu L-Z Mechanistic Insights into the Interface-Directed Transformation of Thiols into Disulfides and Molecular Hydrogen by Visible-Light Irradiation of Quantum Dots. Angew. Chem. Int. Ed 2014, 53, 2085–2089.

57. Zhu X; Lin Y; San Martin J; Sun Y; Zhu D; Yan Y Lead Halide Perovskites for Photocatalytic Organic Synthesis. Nat. Commun 2019, 10, 2843. [PubMed: 31253792]

58. Jones LO; Mosquera MA; Jiang Y; Weiss EA; Schatz GC; Ratner MA Thermodynamics and Mechanism of a Photocatalyzed Stereoselective [2+2] Cycloaddition on a CdSe Quantum Dot. J. Am. Chem. Soc 2020, 142, 15488–15495. [PubMed: 32815721]

59. Jiang Y; López-Arteaga R; Weiss EA Quantum Dots Photocatalyze Intermolecular [2 + 2] Cycloadditions of Aromatic Alkenes Adsorbed to Their Surfaces via van Der Waals Interactions. J. Am. Chem. Soc 2022, 144, 3782–3786. [PubMed: 35230100]

60. Hu H; Chen M; Yao N; Wu L; Zhong Q; Song B; Cao M; Zhang Q Highly Stable CsPbBr3 Colloidal Nanocrystal Clusters as Photocatalysts in Polar Solvents. ACS Appl. Mater. Interfaces 2021, 13, 4017–4025. [PubMed: 33433989]

61. Chauviré T; Mouesca J-M; Gasparutto D; Ravanat J-L; Lebrun C; Gromova M; Jouneau P-H; Chauvin J; Gambarelli S; Maurel V Redox Photocatalysis with Water-Soluble Core–Shell CdSe-ZnS Quantum Dots. J. Phys. Chem. C 2015, 119, 17857–17866.

62. Truesdell BL; Hamby TB; Sevov CS General C(Sp2)–C(Sp3) Cross-Electrophile Coupling Reactions Enabled by Overcharge Protection of Homogeneous Electrocatalysts. J. Am. Chem. Soc 2020, 142, 5884–5893. [PubMed: 32115939]

63. Dabbous A; Colson E; Chakravorty D; Mouesca J-M; Lombard C; Caillat S; Ravanat J-L; Dubois F; Dénès F; Renaud P; Maurel V Fine Tuning of Quantum Dots Photocatalysts for the Synthesis of Tropane Alkaloid Skeletons**. Chem. – Eur. J 2023, 29, e202300303. [PubMed: 36867586]

64. Diroll BT; Guzelturk B; Po H; Dabard C; Fu N; Makke L; Lhuillier E; Ithurria S 2D II–VI Semiconductor Nanoplatelets: From Material Synthesis to Optoelectronic Integration. Chem. Rev 2023, 123, 3543–3624. [PubMed: 36724544]

65. Small differences in the reported oxidation potentials of TEOA (+0.68 V vs SCE), DIPEA (+0.63 V vs SCE), and triethylamine (+0.80 V vs SCE) are inconsistent with their differences in catalytic performance

66. Kamada K; Jung J; Wakabayashi T; Sekizawa K; Sato S; Morikawa T; Fukuzumi S; Saito S Photocatalytic CO2 Reduction Using a Robust Multifunctional Iridium Complex toward the

Selective Formation of Formic Acid. J. Am. Chem. Soc 2020, 142, 10261–10266. [PubMed: 32456417]

67. Chen F; Hu S; Li S; Tang G; Zhao Y Visible-Light-Induced Denitrogenative Phosphorylation of Benzotriazinones: A Metal- and Additive-Free Method for Accessing Ortho-Phosphorylated Benzamide Derivatives. Green Chem 2021, 23, 296–301.
68. Tian H; Shimakoshi H; Park G; Kim S; You Y; Hisaeda Y Photocatalytic Function of the B12 Complex with the Cyclometalated Iridium(Iii) Complex as a Photosensitizer under Visible Light Irradiation. Dalton Trans 2018, 47, 675–683. [PubMed: 29271445]
69. Pal A; Ghosh I; Sapra S; Koenig B Quantum Dots in Visible-Light Photoredox Catalysis: Reductive Dehalogenations and C-H Arylation Reactions Using Aryl Bromides. Chem. Mater 2017, 29, 5225–5231.
70. Objective cost comparisons for photocatalyst use are challenging. Our optimal QDs are not yet commercially available, while the final costs of using molecular photocatalysts depend on catalyst sourcing, loading, and purification considerations. However, the bulk prices of respective precursor materials are illustrative: CdS QDs are produced using CdO ($14/mol, alfa aesar), and sulfur (<1¢/mol). Ir photocatalysts are usually produced from IrCl3 ($57660/mol, Pressure Chemical) and heteroaromatic organic ligands which impart variable synthetic costs. Isophthalonitrile photocatalysts are typically prepared from tetrafluoroisophthalonitrile ($1376/mol, Ambeed) and various aromatic amines. Moreover, CdS QDs can be prepared in a single step and isolated without chromatography
71. Zhang Z; Edme K; Lian S; Weiss EA Enhancing the Rate of Quantum-Dot-Photocatalyzed Carbon–Carbon Coupling by Tuning the Composition of the Dot's Ligand Shell. J. Am. Chem. Soc 2017, 139, 4246–4249. [PubMed: 28290682]
72. Nepomnyashchii AB; Harris RD; Weiss EA Composition and Permeability of Oleate Adlayers of CdS Quantum Dots upon Dilution to Photoluminescence-Relevant Concentrations. Anal. Chem 2016, 88, 3310–3316. [PubMed: 26901485]
73. Weinberg DJ; He C; Weiss EA Control of the Redox Activity of Quantum Dots through Introduction of Fluoroalkanethiolates into Their Ligand Shells. J. Am. Chem. Soc 2016, 138, 2319–2326. [PubMed: 26820492]
74. Chang CM; Orchard KL; Martindale BCM; Reisner E Ligand Removal from CdS Quantum Dots for Enhanced Photocatalytic H2 Generation in PH Neutral Water. J. Mater. Chem. A 2016, 4, 2856–2862.
75. Hassinen A; Moreels I; De Nolf K; Smet PF; Martins JC; Hens Z Short-Chain Alcohols Strip X-Type Ligands and Quench the Luminescence of PbSe and CdSe Quantum Dots, Acetonitrile Does Not. J. Am. Chem. Soc 2012, 134, 20705–20712. [PubMed: 23190352]
76. Owen JS; Park J; Trudeau P-E; Alivisatos AP Reaction Chemistry and Ligand Exchange at Cadmium−Selenide Nanocrystal Surfaces. J. Am. Chem. Soc 2008, 130, 12279–12281. [PubMed: 18722426]
77. Anderson NC; Hendricks MP; Choi JJ; Owen JS Ligand Exchange and the Stoichiometry of Metal Chalcogenide Nanocrystals: Spectroscopic Observation of Facile Metal-Carboxylate Displacement and Binding. J. Am. Chem. Soc 2013, 135, 18536–18548. [PubMed: 24199846]
78. De Roo J; De Keukeleere K; Hens Z; Van Driessche I From Ligands to Binding Motifs and beyond; the Enhanced Versatility of Nanocrystal Surfaces. Dalton Trans 2016, 45, 13277–13283. [PubMed: 27461488]
79. Knauf RR; Lennox JC; Dempsey JL Quantifying Ligand Exchange Reactions at CdSe Nanocrystal Surfaces. Chem. Mater 2016, 28, 4762–4770.
80. Naiini AA; Young V; Verkade JG New Complexes of Triethanolamine (TEA): Novel Structural Features of [Y(TEA)2](ClO4)3•3C5H5N and [Cd(TEA)2](NO3)2. Polyhedron 2014, 14, 393–400.
81. Hartley CL; Kessler ML; Dempsey JL Molecular-Level Insight into Semiconductor Nanocrystal Surfaces. J. Am. Chem. Soc 2021, 143, 1251–1266. [PubMed: 33442974]
82. Hartley CL; Dempsey JL Electron-Promoted X-Type Ligand Displacement at CdSe Quantum Dot Surfaces. Nano Lett 2019, 19, 1151–1157. [PubMed: 30640472]

83. Fritzinger B; Moreels I; Lommens P; Koole R; Hens Z; Martins JC In Situ Observation of Rapid Ligand Exchange in Colloidal Nanocrystal Suspensions Using Transfer NOE Nuclear Magnetic Resonance Spectroscopy. J. Am. Chem. Soc 2009, 131, 3024–3032. [PubMed: 19199431]

84. Das A; Han Z; Haghighi MG; Eisenberg R Photogeneration of Hydrogen from Water Using CdSe Nanocrystals Demonstrating the Importance of Surface Exchange. Proc. Natl. Acad. Sci. U. S. A 2013, 110, 16716. [PubMed: 24082134]

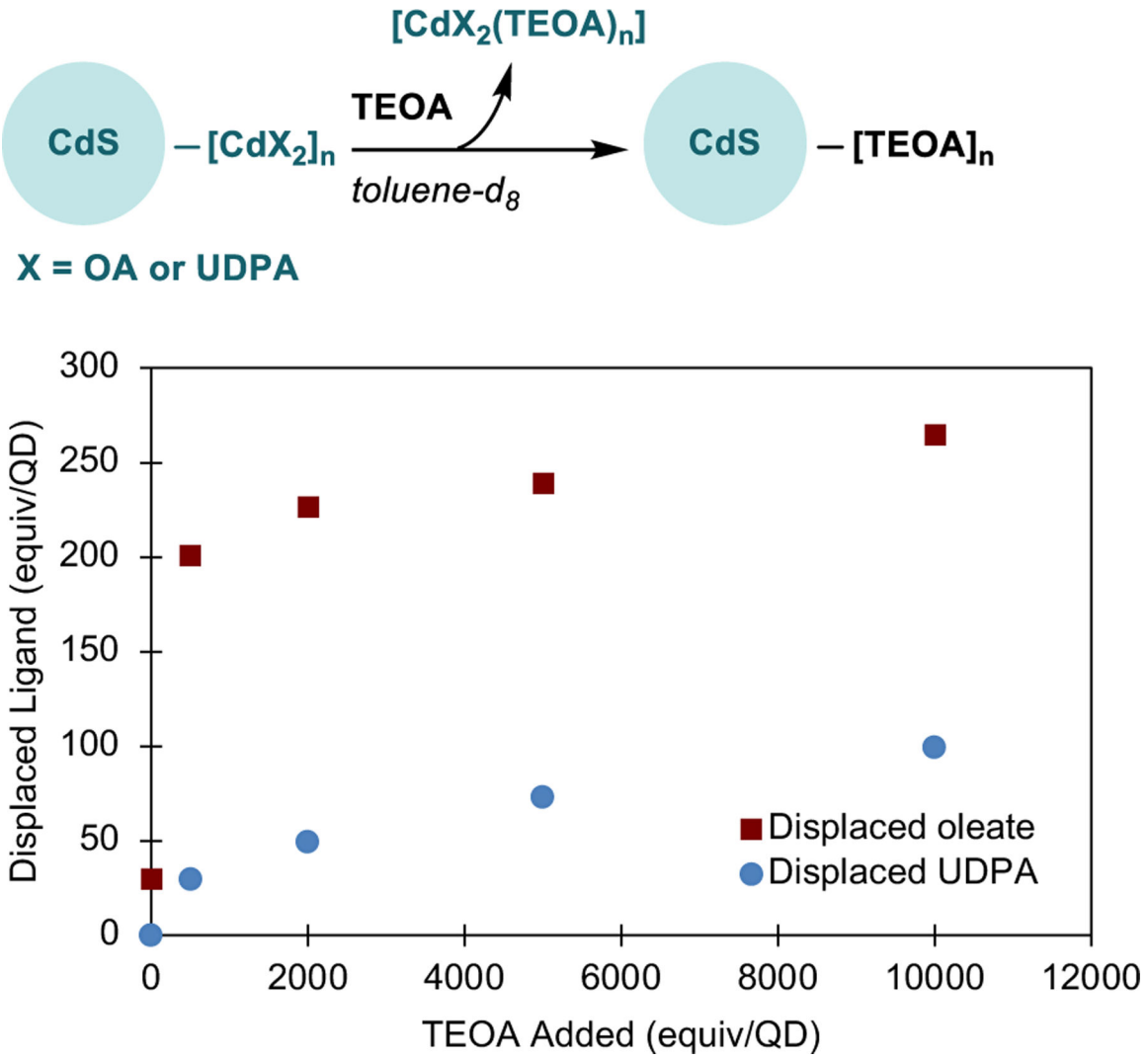

Figure 1.

Displacement of native oleate (OA) ligands and undec-10-en-1-ylphosphonic acid (UDPA) from the surface of CdS QDs after treatment with triethanolamine (TEOA) in toluene-d_8. See Supporting Information Section 4 for experimental details and NMR spectra.

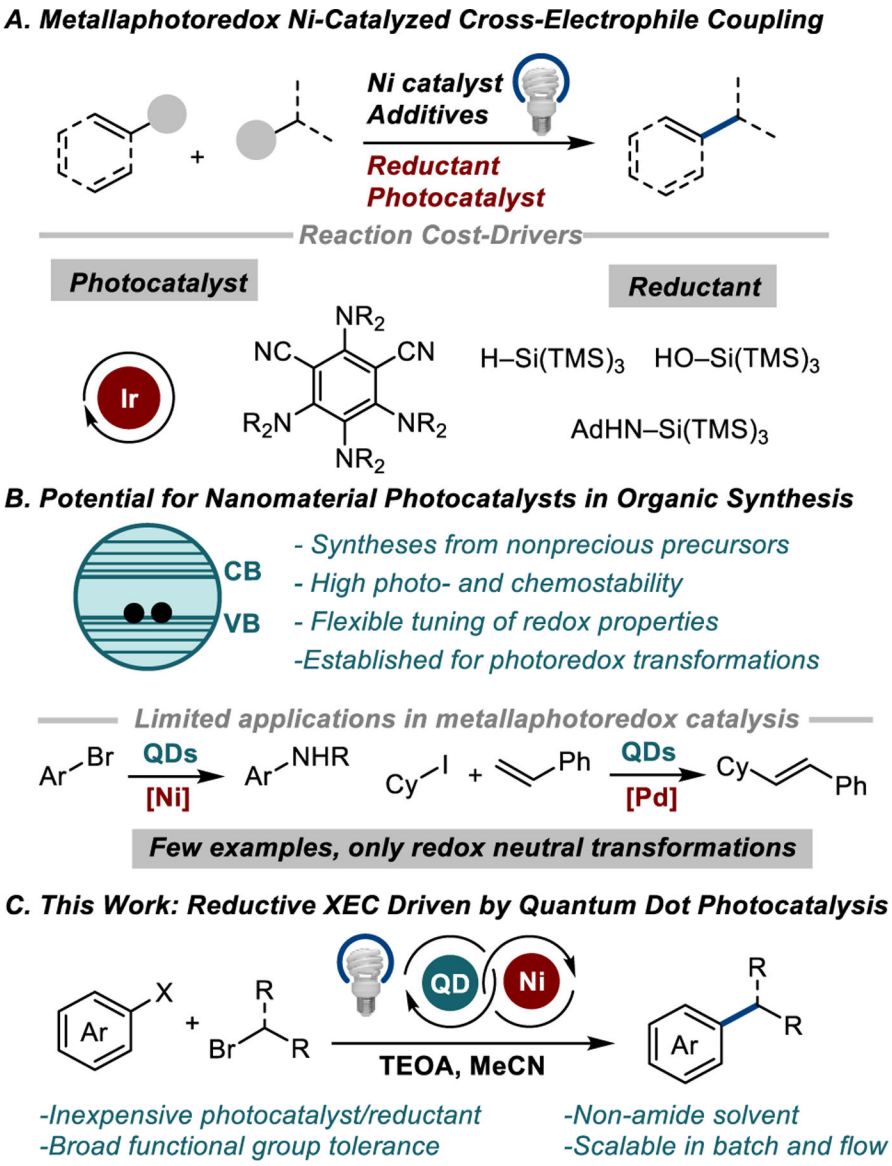

Scheme 1.
Nickel Photoredox Catalysis and Quantum Dots.

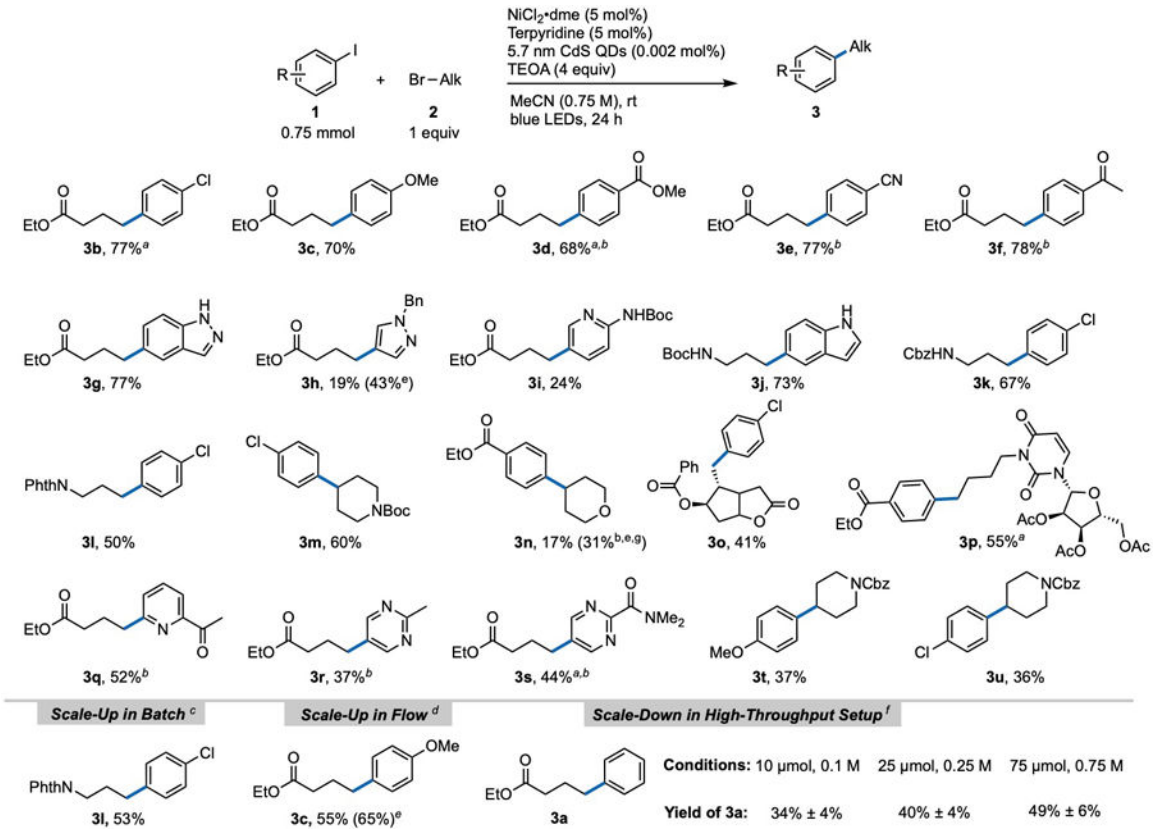

Scheme 2.

QD Promoted Cross-Electrophile Coupling Reaction Scope and Scalability.

Isolated yields after purification unless otherwise noted. See Supporting Information for details. The emission of the blue LEDs was centered around 447 nm. [a]Product could not be fully isolated from impurities, yield determined via ^{1}H NMR spectroscopy. [b]Aryl bromide (1.5 equiv) used instead of aryl iodide. [c]Conducted on 5.0 mmol scale in batch. [d]Conducted on 7.5 mmol scale using a flow setup. [e] ^{1}H NMR yield before purification. [f]Conducted in 100 µL MeCN in a well plate setup. Corrected GC yields. [g] Using 1 equiv of NaI.

Table 1.

Survey of Nanomaterial Photoredox Catalysts.

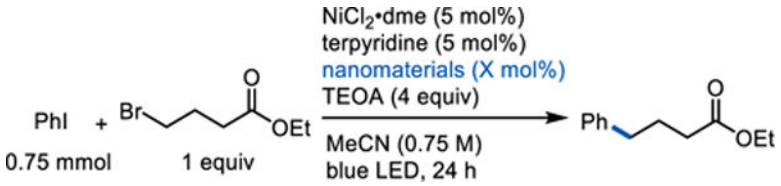

Entry	Nanomaterial Photocatalyst try	Yield (%)[a]
1	7 nm CdS QDs (± 0.72 nm) (2×10^{-3}	79 (80)[b]
2	5.3 nm CdS QDs (2×10^{-3} mol%)	67
3	4.9 nm CdS QDs (2×10^{-3} mol%)	64
4	3.9 nm CdS QDs, (2×10^{-3} mol%)	29
5	5.7 nm CdS QDs, 390 nm hν (2×10^{-3} mol%)	66
6	3.9 nm CdS QDs, 390 nm hν (2×10^{-3} mol%)	21
7	3.0 nm CdSe QDs (2×10^{-3} mol%)	4
8	2.2 nm CdSe QDs (2×10^{-3} mol%)	5
9	$CsPbBr_3$ Bulk Perovskite (10 mol%)	0
10	$CsPbBr_3$ Perovskite QDs (1×10^{-3} mol%)	1
11	4.5-ML CdSe Nanoplatelets (2×10^{-5} mol%)	10[c]
12	4.5-ML CdS Nanoplatelets, 427 nm hν (6×10^{-5} mol%)	35[c]
13	4.5-ML CdS Nanoplatelets, 390 nm hν (6×10^{-5} mol%)	34[c]
14	4.5-ML CdS Nanoplatelets, 390 nm hν (1.4×10^{-4} mol%)	53[c]

Reactions conducted at 0.75 mmol scale using 1 equiv of each coupling partner. The emission of the blue LEDs was centered around 447 nm. Catalyst loading is in mol% of nanomaterial (e.g., QD, platelet).

[a] Corrected GC yields.

[b] Yield determined by ^{1}H NMR.

[c] 48 h reaction time.

Table 2.

Reaction Optimization Studies.

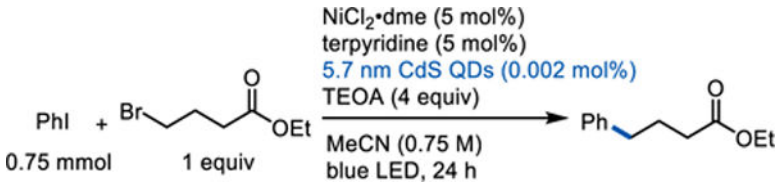

Entry	Variation	Yield (%)[a]
1	None	79 (80)[b]
2	1 mol% [Ni] + ligand	60
3	2.5 equiv TEOA	63
4	Hantzch ester instead of TEOA	ND
4	Et3N instead of TEOA	19
5	DIPEA instead of TEOA	17
6	*N*-ethyldiethanolamine instead of TEOA	63
7	2-diethylaminoethanol instead of TEOA	16
8	2×10^{-4} mol% QDs	36
9	Bulk CdS (10 mol%) instead of QDs	13
10	Omission of any one of Ni, ligand, reductant, light, or QDs	0

Reactions conducted at 0.75 mmol scale using 1 equiv of each coupling partner. The emission of the blue LEDs was centered around 447 nm.

[a]Corrected GC yields.

[b]Yield determined by ^{1}H NMR.